



PCCP

**Kinetic fall-off behavior for the Cl + Furan-2,5-dione
(C₄H₂O₃, maleic anhydride) reaction**

Journal:	<i>Physical Chemistry Chemical Physics</i>
Manuscript ID	CP-ART-12-2020-006402.R1
Article Type:	Paper
Date Submitted by the Author:	08-Feb-2021
Complete List of Authors:	Chattopadhyay, Aparajeo; National Oceanic and Atmospheric Administration Boulder Gierczak, Tomasz; University of Warsaw, Chemistry Marshall, Paul; University of North Texas, Chemistry Papadimitriou, Vassileios C.; Univ Crete Burkholder, James; National Oceanic and Atmospheric Administration (NOAA), Aeronomy Laboratory

SCHOLARONE™
Manuscripts

Kinetic fall-off behavior for the Cl + Furan-2,5-dione (C₄H₂O₃, maleic anhydride) reaction

Aparajeo Chattopadhyay,^{1,2} Tomasz Gierczak,^{1,2} Paul Marshall,^{1,2,3} Vassileios C. Papadimitriou,^{1,2} and James B. Burkholder^{1,*}

¹ Chemical Sciences Laboratory, National Oceanic and Atmospheric Administration, 325 Broadway, Boulder, CO, USA 80305-3327

² Cooperative Institute for Research in Environmental Sciences, University of Colorado, Boulder, CO, USA 80309

³ Department of Chemistry and Center for Advanced Scientific Computing and Modeling, University of North Texas, 1155 Union Circle #305070, Denton, Texas 76203, USA.

*Correspondence

James B. Burkholder

Chemical Sciences Laboratory,

National Oceanic and Atmospheric Administration,

325 Broadway, Boulder, CO 80305-3327

Ph: 303-497-3252

Email: James.B.Burkholder@noaa.gov

Abstract

Rate coefficients, k , for the gas-phase Cl + Furan-2,5-dione ($C_4H_2O_3$, maleic anhydride) reaction were measured over the 15–500 Torr (He and N_2 bath gas) pressure range at temperatures between 283 and 323 K. Kinetic measurements were performed using pulsed laser photolysis (PLP) to produce Cl atoms and atomic resonance fluorescence (RF) to monitor the Cl atom temporal profile. Complementary relative rate (RR) measurements were performed at 296 K and 620 Torr pressure (syn. air) and found to be in good agreement with the absolute measurements. A Troe-type fall-off fit of the temperature and pressure dependence yielded the following rate coefficient parameters:

$$k_0(T) = (9.4 \pm 0.5) \times 10^{-29} (T/298)^{-6.3} \quad \text{cm}^6 \text{ molecule}^{-2} \text{ s}^{-1}$$

$$k_\infty(T) = (3.4 \pm 0.5) \times 10^{-11} (T/298)^{-1.4} \quad \text{cm}^3 \text{ molecule}^{-1} \text{ s}^{-1}$$

The formation of a $Cl \bullet C_4H_2O_3$ adduct intermediate was deduced from the Cl atom temporal profiles and an equilibrium constant, $K_p(T)$, for the $Cl + C_4H_2O_3 \leftrightarrow Cl \bullet C_4H_2O_3$ reaction was determined. A third-law analysis yielded $\Delta H = -15.7 \pm 0.4 \text{ kcal mol}^{-1}$ with $\Delta S = -25.1 \text{ cal K}^{-1} \text{ mol}^{-1}$, where ΔS was derived from theoretical calculations at the B3LYP/6-311G(2d,p,d) level. In addition, the rate coefficient for the $Cl \bullet C_4H_2O_3 + O_2$ reaction at 296 K was measured to be $(2.83 \pm 0.16) \times 10^{-12} \text{ cm}^3 \text{ molecule}^{-1} \text{ s}^{-1}$, where the quoted uncertainty is the 2σ fit precision. Stable end-product molar yields of (83 ± 7) , (188 ± 10) , and $(65 \pm 10)\%$ were measured for CO, CO_2 , and HC(O)Cl, respectively, in an air bath gas. An atmospheric degradation mechanism for $C_4H_2O_3$ is proposed based on the observed product yields and theoretical calculations of ring-opening pathways and activation barrier energies at the CBS-QB3 level of theory.

Introduction

Furan-2,5-dione ($C_4H_2O_3$, maleic anhydride (MA)) is an unsaturated oxygenated cyclic compound that has biomass burning¹⁻⁵ as well as anthropogenic⁶⁻⁹ atmospheric sources. In biomass burning, maleic anhydride emission¹⁻⁴ has been associated with the oxidation of furan and its substituted derivatives, e.g. 2,5-methyl furan and furfural^{1,10-12} and may serve as a tracer for biomass burning plume chemistry. The emission of MA potentially impacts local and regional air quality and human health through degradation mechanisms that lead to the formation of ozone and secondary organic aerosol. A quantitative understanding of the atmospheric fate of MA and its degradation products is desired for improved air quality forecast modeling.

Maleic anhydride is removed from the atmosphere via gas-phase reaction with the atmospheric oxidants Cl, OH, NO_3 , and O_3 , by UV photolysis,¹³ and via wet/dry deposition. Presently, the atmospheric chemistry of MA is understudied and a recent study from this laboratory,¹⁴ reported the OH radical reaction:



rate coefficient, k , and its temperature dependence to be $k_1(283\text{--}374\text{ K}) = (1.55 \pm 0.20) \times 10^{-12} \exp(-410 \pm 44/T) \text{ cm}^3 \text{ molecule}^{-1} \text{ s}^{-1}$ and $k_1(296\text{ K}) = (3.93 \pm 0.28) \times 10^{-13} \text{ cm}^3 \text{ molecule}^{-1} \text{ s}^{-1}$. This result implies an atmospheric lifetime of ~ 15 days with respect to loss via reaction with the OH radical. To the best of our knowledge, rate coefficient data for other atmospheric oxidant reactions have not been reported to date. The OH and Cl atom reactions are expected to proceed through an addition mechanism to form an adduct intermediate that under atmospheric conditions will be rapidly converted to a peroxy radical via reaction with O_2 . The subsequent atmospheric chemistry of the peroxy radical is presently not well established, but will most likely involve reaction with NO or HO_2 leading to ring opening reaction pathways and the formation of stable end-products.

In this study, the temperature and pressure dependence of the Cl atom reaction:



was measured using a pulsed laser photolysis – resonance fluorescence (PLP-RF) technique. A complementary relative rate kinetic measurement was also performed as part of this study. In addition, stable end-products were measured following reaction 2 under NO_x ($NO_x = NO + NO_2$) free conditions. An atmospheric degradation mechanism is proposed that is consistent with the observed reaction end-products and theoretical calculations of ring-opening pathways and activation energies of reaction steps at the CBS-QB3 level of theory.

Experimental details

Rate coefficients for reaction 2 were measured between 283 and 323 K at total pressures in the 15 to 500 Torr range (He and N₂ bath gases) using a pulsed laser photolysis (PLP) – resonance fluorescence (RF) method. Rate coefficients were also measured using a relative rate (RR) method at 296 K and 620 Torr (syn. air) total pressure. Stable end-product yields were measured as part of the RR experiments. The experimental apparatus and methods used in the kinetic and product yield measurements are described separately below.

Pulsed laser photolysis – resonance fluorescence (PLP–RF) method

The PLP–RF apparatus has been used previously in our laboratory^{15,16} and is only described briefly here. Experiments were performed under slow-flow conditions under pseudo first-order conditions in Cl, i.e., [C₄H₂O₃] >>[Cl].

The multi-port small volume (~250 cm³) jacketed Pyrex RF reactor had a solar blind photomultiplier tube (PMT, 115–200 nm sensitivity) mounted orthogonal to the resonance lamp and the photolysis laser beam paths. The reactor temperature was controlled by circulating fluid from a temperature-regulated reservoir through its jacket and the temperature of the gas in the reaction zone (the intersection of the photolysis and the resonance lamp beams) was measured with a retractable thermocouple to within 1 K. Cl atom temporal profiles (fluorescence at 134.73 and 136.35 nm) were recorded in 5 or 10 μs bins beginning 1 ms prior to the photolysis laser pulse. Temporal profiles were co-added to improve the signal-to-noise (S/N) with 2000 profiles typically being co-added. The background signal, due primarily to scattered light from the resonance lamp, was measured in the 1 ms prior to the photolysis laser pulse.

The atomic resonance lamp had a CaF₂ window and was powered with a 20 W microwave cavity. The lamp was operated at ~2.8 Torr with a small flow of a 3% Cl₂ in He mixture diluted with additional He gas flow. The Cl detection limit (S/N = 1) was determined to be ~5 × 10⁸ and ~5 × 10⁹ atom cm⁻³ for 1 s integration in 100 Torr He and N₂ bath gas, respectively.

Cl radicals were produced by 351 nm (XeF excimer laser) pulsed laser photolysis of Cl₂:



The initial Cl radical concentration, [Cl]₀, was estimated from [Cl₂], the Cl₂ absorption cross section at 351 nm, and the photolysis laser fluence measured at the exit of the reactor with a power meter. The photolysis laser fluence was varied in the range ~2–8 mJ cm⁻² pulse⁻¹ over the course

of the study. The Cl_2 concentration in the reactor was determined from the flow of a 3% Cl_2/He mixture, the total gas flow, and reactor pressure. $[\text{Cl}_2]$ was in the range $\sim(3\text{--}37) \times 10^{14}$ molecule cm^{-3} corresponding to $[\text{Cl}]_0$ in the range $(1.2\text{--}7.0) \times 10^{12}$ molecule cm^{-3} . The laser repetition rate was between 4–5 Hz, which ensured a fresh gas sample for each photolysis laser pulse for the linear gas flow rates through the reactor, 4–22 cm s^{-1} , used in this work.

The MA concentration was measured on line by infrared (500–4000 cm^{-1}) and UV (213.9 nm) absorption. Infrared absorption measurements were made after the reactor using a Fourier transform infrared (FTIR) spectrometer equipped with a multi-pass absorption cell (485 cm total pathlength). The detector was a liquid N_2 cooled HgCdTe/B semiconductor. Spectra were recorded at a spectral resolution of 1 cm^{-1} . The MA absorption was quantified using an integrated band strength of 9.00×10^{-17} cm^2 molecule $^{-1}$ for the 1700–2000 cm^{-1} region measured previously in this laboratory.¹³ The UV absorption measurement was performed before the gas flow entered the reactor. The setup consisted of a 20 cm long Pyrex absorption cell (1.9 cm i.d.) with quartz windows, a Zn Pen-ray lamp light source, and a photodiode detector with a 213.9 nm bandpass filter. A separate photodiode detector was used to continuously monitor the stability of the light source before passing through the absorption cell. The 213.9 nm absorption cross section of MA was taken from our previous study, 3.06×10^{-17} cm^2 molecule $^{-1}$.¹³ The $\text{C}_4\text{H}_2\text{O}_3$ concentrations determined from the UV and infrared absorption measurements were scaled to account for the differences in pressure and temperature between the room temperature absorption cells and the reactor.

The Cl atom temporal profiles are described by:



where $\text{Cl}\cdot\text{C}_4\text{H}_2\text{O}_3$ represents an adduct reaction intermediate. At low temperature, the $\text{Cl}\cdot\text{C}_4\text{H}_2\text{O}_3$ adduct is stable and exponential Cl atom decay profiles are expected. At elevated temperatures, reaction 2b, i.e., the thermal decomposition of the $\text{Cl}\cdot\text{C}_4\text{H}_2\text{O}_3$ adduct back to reactants, becomes more rapid and at sufficiently high temperatures leads to rapid equilibration and no apparent subsequent loss of Cl atom. At intermediate temperatures, the Cl atom temporal profiles display an approach to equilibrium with background loss of Cl and $\text{Cl}\cdot\text{C}_4\text{H}_2\text{O}_3$ observed at longer reaction times:



Under these conditions the Cl atom temporal profile is described by:¹⁷

$$(S_t/S_0) = \{(Q + \lambda_1) \exp(\lambda_1 t) - (Q + \lambda_2) \exp(\lambda_2 t)\} / (\lambda_1 - \lambda_2) \quad (\text{I})$$

where S_t and S_0 are the resonance fluorescence signal levels at times t and 0 , and

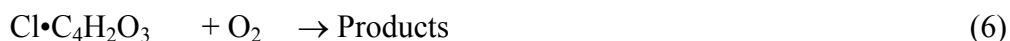
$$Q = k_r + k_{\text{Loss}} \quad (\text{II})$$

$$Q + k_d + k_f[\text{C}_4\text{H}_2\text{O}_3] = -(\lambda_1 + \lambda_2) \quad (\text{III})$$

$$k_d Q + k_{\text{Loss}} k_f[\text{C}_4\text{H}_2\text{O}_3] = \lambda_1 \lambda_2 \quad (\text{IV})$$

k_d was measured in the absence of MA in separate experiments at the beginning and end of each experiment. Values of k_d were in the 6–250 s^{-1} range. Cl atom temporal profiles obtained between 283 and 323 K displayed the approach to equilibrium profile and were fit to eq. I using a non-linear least-squares method. At temperatures less than 283 K, reliable rate coefficient data was not obtained due primarily to uncertainty in the MA concentration. At temperatures greater than ~335 K, thermal decomposition of the $\text{Cl}\cdot\text{C}_4\text{H}_2\text{O}_3$ adduct was too rapid to enable an accurate determination of k_f .

k_{Loss} most likely represents reaction of the $\text{Cl}\cdot\text{C}_4\text{H}_2\text{O}_3$ adduct with O_2 impurities in the bath gas:



and diffusion out of the detection volume. k_{Loss} varied with total pressure and temperature with typical values in the 100–200 s^{-1} range, although several experiments had greater values. As part of this study, $k_6(296 \text{ K})$ was determined by adding known amounts of O_2 to the reaction mixture, with other conditions held constant and measuring the increase in k_{Loss} .

Relative rate method

The relative rate apparatus consists of (1) a 100 cm long Pyrex cylinder (~250 cm^3), (2) a pulsed excimer laser photolysis source used to produce Cl atoms, (3) a Fourier transform infrared spectrometer (FTIR) used to monitor the reactant and product concentrations, and (4) a Teflon diaphragm pump used to circulate the reaction mixture between the reactor and the FTIR absorption cell.

The photolysis laser beam passed along the length of the reactor and Cl atoms were produced via either 248 nm pulsed laser photolysis of oxalyl chloride, $\text{C}_2\text{O}_2\text{Cl}_2$:



or 351 nm pulsed laser photolysis of Cl_2 (reaction 3). The 248 nm photolysis experiments were complicated by the photodissociation of MA and, although consistent with the Cl_2 photolysis experiments, were less accurate and are not presented here. The 351 nm photolysis laser fluence

was in the 3–4 mJ cm⁻² pulse⁻¹ range over the course of the study and the laser repetition rate was 20 Hz. The residence time of the gas in the reactor was ~6 s. Experiments were performed at a total pressure of ~620 Torr with syn. air bath gas. The initial C₄H₂O₃ concentration was in the range (8.7–23.4) × 10¹⁴ molecule cm⁻³.

Kinetic data were also obtained using a conventional relative rate method in which the loss of MA was measured relative to the loss of a reference compound:

$$\ln \left(\frac{[\text{MA}]_0}{[\text{MA}]_t} \right) - k_w t = \frac{k_2}{k_{\text{ref}}} \ln \left(\frac{[\text{ref}]_0}{[\text{ref}]_t} \right) \quad (\text{V})$$

where [MA]₀ and [ref]₀ are the initial concentrations of MA and reference compound, respectively, [MA]_t and [ref]_t are the concentrations at time t, and k_{ref} is the rate coefficient for the reaction of the reference compound. k_wt represents the dark background loss of MA, which was measured in separate experiments. C₂H₆ and C₂H₄ were used as reference compounds in this study:



where k₈(298 K) = 5.70 × 10⁻¹¹ cm³ molecule⁻¹ s⁻¹ and k₉(298 K) = 9.78 × 10⁻¹¹ cm³ molecule⁻¹ s⁻¹.¹⁸ FTIR absorption measurements were used to monitor the loss of MA and the reference compounds. A time zero infrared spectrum was recorded (1 cm⁻¹ resolution, 500 and 4000 cm⁻¹ in 10 co-adds (~10 s total time) after the gases were mixed for ~2 mins. The gas mixture was then exposed to the photolysis laser and infrared spectra were recorded in rapid succession automatically. A complete experiment was completed in less than 180 s. Stable end-products (CO, CO₂, and HC(O)Cl) were identified via infrared absorption and quantified using standard reference spectra. Stable end-product measurements were performed under similar conditions to the relative rate experiments, but without the addition of a reference compound.

Materials

He (UHP, 99.999 %), N₂ (UHP, 99.99%), O₂ (UHP, 99.99%), zero air, and a commercial 3% Cl₂ in He mixture were used as supplied. C₄H₂O₃ (>99.0%, Furan-2,5-dione, CAS RN: 108-31-6), a solid at room temperature, was stored in a Pyrex vacuum reservoir at room temperature and its vapor swept into the PLP–RF and RR apparatus by passing a flow of bath gas (He or N₂) over the solid sample. The MA concentration in the PLP–RF reactor was varied by varying the fraction of the total flow passing through the reservoir. Gas flows were measured with calibrated mass flow

meters and pressures were measured using capacitance manometers. Uncertainties quoted herein are 2σ unless noted otherwise.

Theoretical methods

Molecular structures were optimized using density functional theory at the B3LYP/6-311G(2d,p,d) level, along with harmonic vibrational frequencies. These were scaled by a standard factor of 0.99 to approximate fundamental frequencies.¹⁹ These data, plus the empirical electronic partition function for Cl atoms,²⁰ were employed to derive²¹ the entropy change for the addition process 2a. Next, electronic energies were obtained via the CBS-QB3 methodology, which approximates an extrapolation of coupled-cluster results to the complete basis set limit.¹⁹ All calculations were made with the Gaussian16 program suite.²² The energy of atomic Cl was corrected by $-0.8 \text{ kcal mol}^{-1}$ to account for the influence of the $^2P_{3/2}$ and $^2P_{1/2}$ electronic states.²⁰ Possible intermediates in subsequent reactions of the Cl/MA system and connecting transition states were explored with the same computational approach, to derive reaction barriers at 0 K. The possible uncertainty in the relative energies based on CBS-QB3 theory is up to $2\text{-}3 \text{ kcal mol}^{-1}$.²³

Results and discussion

The kinetic results obtained in the absolute and relative rate coefficient for the Cl + MA reaction, $k_2(T,P)$, the equilibrium constant for the forward and reverse of reaction 2, and the Cl•C₄H₂O₃ adduct + O₂ rate coefficient are presented separately below. Subsequently, a reaction mechanism that is supported by the observed stable end-product yields and theoretical calculations for the reaction pathways is proposed.

PLP-RF Rate Coefficient Measurement

Absolute $k_2(T,P)$ measurements were performed using the PLP–RF method for temperatures in the range 283 to 323 K at total pressures between 15 and 500 Torr (N₂ bath gas). Kinetic data was also obtained between 50 and 500 Torr with He as the bath gas at 296, 308, and 323 K.

Figure 1 shows a representative set of Cl atom temporal profiles obtained at 296 K and 100 Torr (N₂). The measured profiles clearly show bi-exponential behavior consistent with Cl atom regeneration, i.e., the formation and decomposition of a Cl•C₄H₂O₃ adduct. The profiles observed at higher temperature show a more rapid approach toward equilibrium. At longer reaction times, the loss of the Cl atom signal is due to Cl atom and Cl•C₄H₂O₃ adduct losses, k_d and k_{Loss} . The data obtained at 283, 308, and 323 K are of similar quality to that shown in **Figure 1** and

representative data are plotted in the supporting information, **Figures S1-S3**. **Figure 1** includes the non-linear least-squares fits of the Cl atom temporal profiles to equation 1, which reproduce the experimental data to within the measurement precision. **Tables S1** and **S2** provide the detailed fit results for all experiments. **Tables 1** and **2** provide summaries of the experimental conditions and rate coefficients obtained for $k_f(T,P)$, the forward reaction. The $k_f(T,P)$ fit precision is in the range 1–7%. The precision of the $k_r(T,P)$ was more dependent on the experimental conditions as given in **Table S1**.

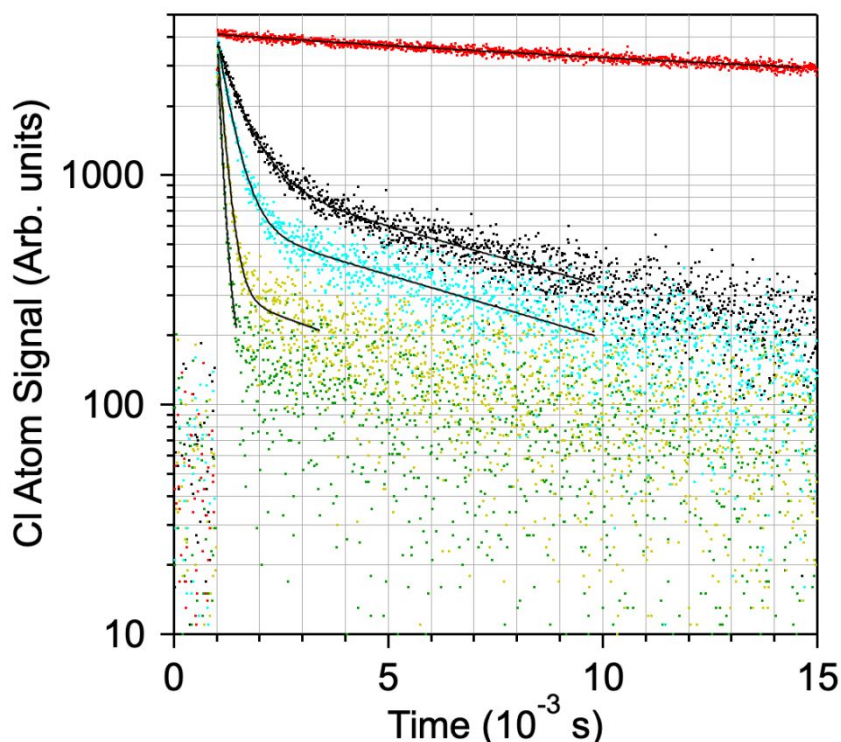


Fig. 1. Representative Cl atom temporal profiles obtained for a range of $C_4H_2O_3$ (MA) concentrations at 296 K and 100 Torr (N_2). MA concentrations from top to bottom profile are (10^{14} molecule cm^{-3}): 0, 0.52, 1.00, 2.16, 3.68 (see **Table 1**). Not all measured Cl atom profiles are shown for improved clarity. The lines for the MA concentration profiles are non-linear least-squares fits of the data to equation I. Representative profiles measured at other temperature are provided in the supporting information.

The kinetic results were independent of experimental parameters such as photolysis laser fluence, Cl_2 concentration, $[Cl]_0$, and gas flow velocity. Measurements of the $C_4H_2O_3$ concentration before and after the reactor agreed to within 1–3%, under all experimental conditions, which demonstrated that there was no loss of $C_4H_2O_3$ through the reactor. In one experiment, 2.2 Torr of O_2 was added to the reaction mixture to act as a $Cl \cdot C_4H_2O_3$ adduct

scavenger. The results obtained for $k_f(T,P)$ in the presence and absence of added O_2 agreed to within the measurement precision, this includes measurements of the $Cl \cdot C_4H_2O_3 + O_2$ rate coefficient presented later. In addition, no measurable dependence of $k_f(T,P)$ was observed in experiments performed using a range of Cl_2 concentrations.

Table 1 Summary of experimental conditions and rate coefficients obtained for the $Cl + C_4H_2O_3 + M (N_2)$ reaction in this work using the PLP–RF method

Temperature (K)	[M] (10^{18} molecule cm^{-3})	Linear gas flow velocity ($cm s^{-1}$)	Photolysis laser fluence ($mJ cm^{-2} pulse^{-1}$)	$[C_4H_2O_3]$ (10^{14} molecule cm^{-3})	k_f^* ($10^{-11} cm^3 molecule^{-1} s^{-1}$)
323	5.94	15.9	2.8	1.10–3.27	2.22 ± 0.08
	2.95	12.5	6.1	0.41–3.51	1.79 ± 0.12
	1.48	17.8	5.0	0.43–5.39	1.41 ± 0.06
	1.49	19.7	2.8	0.99–4.02	1.34 ± 0.09
	0.74	9.3	5.0	0.98–7.72	1.10 ± 0.06
	0.44	5.9	5.5	2.47–15.6	0.849 ± 0.06
308	15.5	3.7	7.2	0.50–2.24	2.75 ± 0.09
	6.19	8.7	7.2	0.18–2.42	2.54 ± 0.06
	3.10	15.6	7.5	0.37–4.65	2.19 ± 0.11
	1.55	20.1	7.5	0.57–2.63	1.79 ± 0.04
	0.77	12.2	8.0	0.76–3.69	1.39 ± 0.04
	0.46	3.7	8.0	1.20–8.80	1.10 ± 0.04
296	16.2	8.6	2.4	0.96–3.42	2.97 ± 0.06
	6.48	11.7	2.0	1.68–5.36	2.74 ± 0.07
	3.24	15.9	4.6	0.52–6.58	2.43 ± 0.04
	3.24	12.9	5.6	1.05–5.62	2.35 ± 0.04
	1.62	22.2	4.6	0.92–2.60	2.01 ± 0.02
	0.81	12.6	2.4	0.85–4.25	1.50 ± 0.02
	0.49	7.9	2.4	1.60–5.39	1.22 ± 0.06
283	16.9	11.4	2.9	1.61–2.99	3.53 ± 0.19
	6.78	13.3	3.0	0.55–3.22	3.13 ± 0.11
	3.39	15.2	3.7	0.83–3.73	2.76 ± 0.06
	1.69	22.1	2.5	0.65–3.06	2.43 ± 0.08
	0.85	13.7	3.0	0.82–3.96	1.95 ± 0.12
	0.51	7.2	2.8	0.75–2.38	1.58 ± 0.03

*Uncertainties are the 2σ precision of the least-squares fit

Table 2 Summary of experimental conditions and rate coefficients obtained for the $Cl + C_4H_2O_3 + M (He)$ reaction in this work using the PLP–RF method

Temperature (K)	[M] (10^{18} molecule cm^{-3})	Linear gas flow velocity ($cm s^{-1}$)	Photolysis laser fluence ($mJ cm^{-2} pulse^{-1}$)	$[C_4H_2O_3]$ (10^{14} molecule cm^{-3})	k_f^* ($10^{-11} cm^3 molecule^{-1} s^{-1}$)
323	2.97	18.7	6.5	0.55–3.63	1.27 ± 0.06
	8.91	6.2	6.8	0.76–3.58	1.91 ± 0.10
308	3.11	17.5	6.0	0.66–5.49	1.53 ± 0.04
296	3.24 ^s	16.0	6.9	1.03–9.30	1.51 ± 0.04
	3.24	16.3	6.5	0.97–9.12	1.55 ± 0.02
	3.24	13.3	7.2	0.41–3.03	1.68 ± 0.06
	3.24	17.5	5.5	0.95–4.43	1.73 ± 0.05
	1.62	24.1	6.2	0.41–3.94	1.29 ± 0.04
	9.72	6.2	6.6	0.58–3.64	2.44 ± 0.04
	16.2	4.5	5.5	0.28–2.49	2.82 ± 0.10

* Uncertainties are the 2σ precision of the least-squares fit.; ^s 2.2 Torr of O_2 added to the reaction mixture.

Figures 2 and S4 for N₂ and He bath gases, respectively, provide a graphical summary of the obtained $k_f(T,P)$ values listed in **Tables 1 and 2**. A non-linear least-squares fit to the N₂ bath gas data set to the Troe fall-off formulation, with $F_c = 0.6$, yielded the following rate coefficient parameters:

$$k_0(T) = (9.4 \pm 0.5) \times 10^{-29} (T/298)^{-6.3} \quad \text{cm}^6 \text{ molecule}^{-2} \text{ s}^{-1}$$

$$k_\infty(T) = (3.4 \pm 0.5) \times 10^{-11} (T/298)^{-1.4} \quad \text{cm}^3 \text{ molecule}^{-1} \text{ s}^{-1}$$

The fit results are included in **Figure 2** and reproduce the experimental data very well for all experimental conditions, with an average deviation of 3%. The uncertainties were estimated based on reasonable fits to the experimental data.

The kinetic data obtained with He bath gas shown in **Figure S4** was fit with a collision efficiency ratio, $\frac{\beta_{He}}{\beta_{N_2}}$, of 0.34, where β_{He} and β_{N_2} are the collision efficiency factors for He and N₂ bath gases, respectively. The fit reproduces the limited He experimental dataset to within the measurement precision.

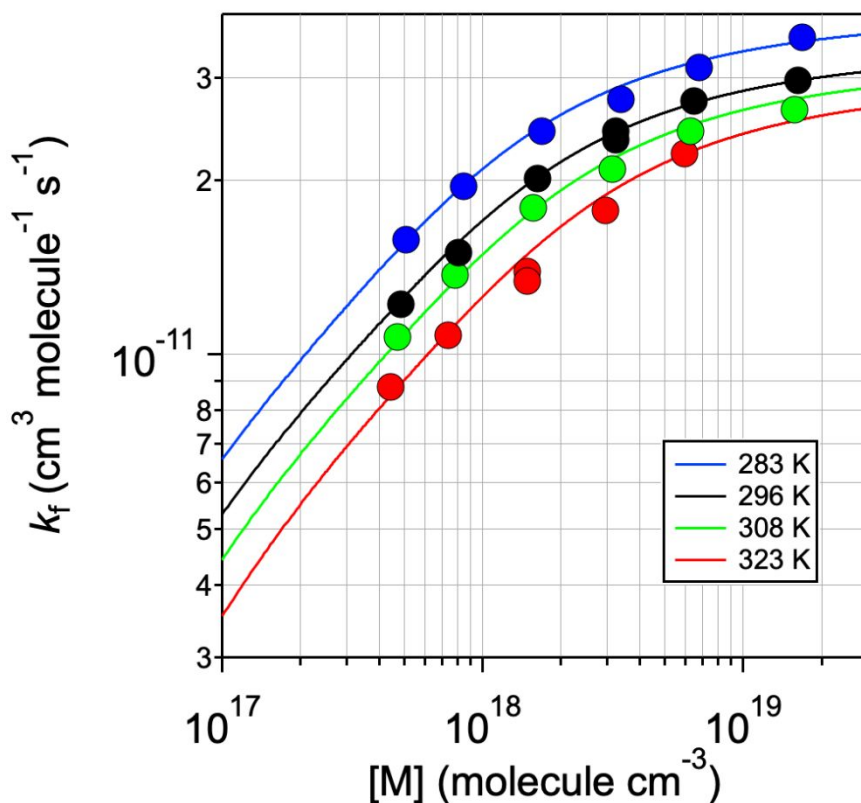


Fig. 2. Rate coefficient data obtained in this work for the Cl + C₄H₂O₃ (MA) + M (N₂) reaction (see **Table 1**). The lines are a non-linear multi-variant least-squares fit of the experimental data to the Troe fall-off formulation (see text).

There are no previous kinetic studies of reaction 2 to compare with the present results. In fact, there is a general lack of experimental kinetic data for anhydrides available in the current literature. The observed fall-off behavior is consistent with an addition reaction, while the high-pressure rate coefficient for reaction 2 is significantly less, by a factor of 3, or more, than that observed for linear, e.g. ethylene and propene,^{18,24} and cyclic, e.g. cyclo-pentene, -hexene, and -heptene,²⁵ unsaturated hydrocarbons.

Relative Rate Coefficient Measurement

Figure 3 shows the results obtained in the relative rate (RR) measurements of reaction 2 at 296 K and 620 Torr (syn. Air). In the RR experiments, it was necessary to account for the dark background loss of MA. Although the experiments were performed on a short time scale (<3 mins.) to minimize the correction, the dark loss corrections still needed to be accounted for in the data analysis. The dark loss of MA was determined in independent measurements under identical conditions, but without photolysis, prior to each kinetic experiment and applied in the RR kinetic data analysis. MA loss measured before and after a RR measurement agreed to within 3%. Results from a background MA loss experiment are shown in **Figure S5**. **Figure 3** includes the uncorrected and corrected data points, where the correction was typically ~25–35%. The precision for measured changes in MA, C₂H₆, and C₂H₄ are estimated to be better than 3, 5, and 5%, respectively.

The data shows the precision of the experimental data and the linear relationship between MA and reference compound loss. Linear least-squares fits of the data yield rate coefficient ratios of 0.48 ± 0.02 and 0.31 ± 0.01 for C₂H₆ and C₂H₄, respectively, where the quoted uncertainties are the fit precision. Using k_{ref} values¹⁸ of $5.70 \times 10^{-11} \text{ cm}^3 \text{ molecule}^{-1} \text{ s}^{-1}$ and $9.78 \times 10^{-11} \text{ cm}^3 \text{ molecule}^{-1} \text{ s}^{-1}$ at 296 K and 620 Torr pressure for C₂H₆ and C₂H₄, respectively, yield $k_2(296 \text{ K})$ values of $(2.74 \pm 0.11) \times 10^{-11} \text{ cm}^3 \text{ molecule}^{-1} \text{ s}^{-1}$ and $(3.00 \pm 0.10) \times 10^{-11} \text{ cm}^3 \text{ molecule}^{-1} \text{ s}^{-1}$. The agreement between the results obtained with the two reference compounds is ~9%, while the data measured using C₂H₄ agrees with the absolute PLP–RF results to within 1%. In this work, the rate coefficients measured using the PLP–RF method are expected to be more accurate than the RR method. The agreement between the PLP–RF and RR results at 296 K for similar total pressure provides additional validation of the PLP–RF results.

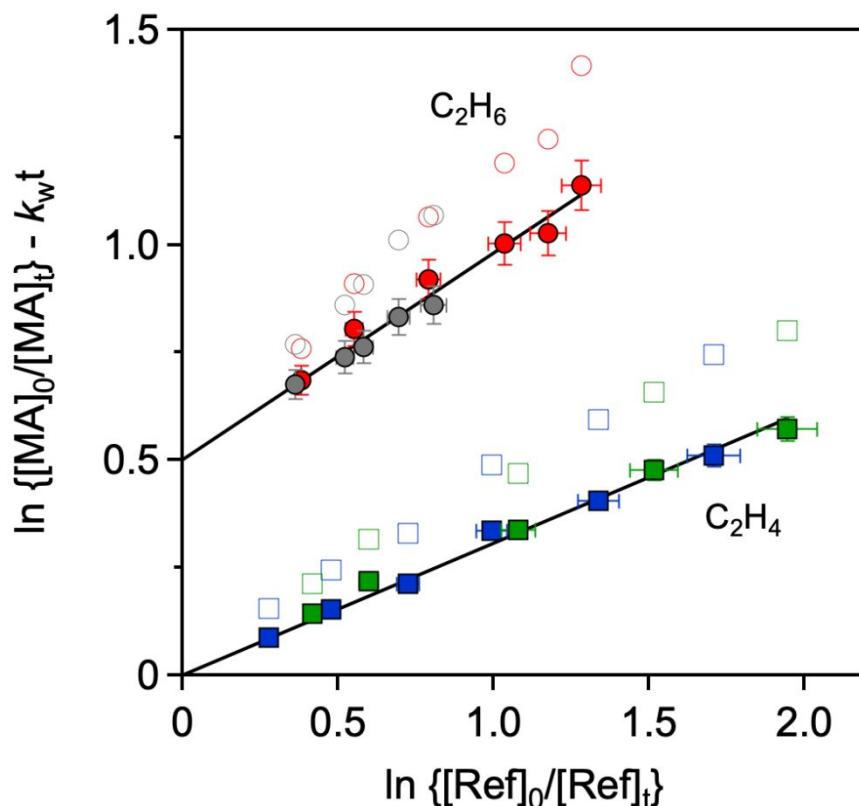


Fig. 3. Relative rate data obtained at 296 K and 620 Torr (syn. air) for the $\text{Cl} + \text{C}_4\text{H}_2\text{O}_3$ (MA) reaction with C_2H_6 and C_2H_4 reference compounds. The data for C_2H_6 reference compound has been offset vertically for clarity. Independent measurements performed under different experimental conditions are represented by different colored symbols. Raw data points are given as open symbols, while the data corrected for background MA loss are given with solid symbols. The data point error bars are from the precision of the measurement. The lines are linear least-squares fits of the combined data for each reference compound.

Equilibrium constant and thermochemistry

Analysis of the Cl atom temporal profiles yields the forward and reverse rate coefficients for reaction 2 and, thus, the equilibrium constant, $K_p(T)$, for the $\text{Cl}\cdot\text{C}_4\text{H}_2\text{O}_3$ adduct formation. The equilibrium constants obtained for all the experiments is given in **Tables S1** and **S2** for N_2 and He bath gas, respectively. Measurements performed at different total pressure and with N_2 and He bath gas yielded consistent $K_p(T)$ values at a given temperature, to within 3–15% for the temperature range 296–323 K, while the uncertainty is greater for the 283 K data due to lower k_r values. The $K_p(T)$ results are summarized in **Table 3** and plotted in **Figure 4**.

Table 3 Summary of $\text{Cl} + \text{C}_4\text{H}_2\text{O}_3 \leftrightarrow \text{Cl}\cdot\text{C}_4\text{H}_2\text{O}_3$ (adduct) equilibrium constant experimental and theoretical data obtained in this work a

Temperature (K)	$K_p(T)$ (10^6 atm^{-1})	
	Theoretical	Experimental ^b
283	159	4.16 ± 0.49
296	39.9	1.41 ± 0.06
308	12.3	0.57 ± 0.02
323	3.2	0.17 ± 0.01

^a K_p values (in atm^{-1}) were obtained by multiplying K_c by $(6.023 \times 10^{23})/(82.06 \times T)$; ^b Estimated uncertainties are the 2σ fit precision

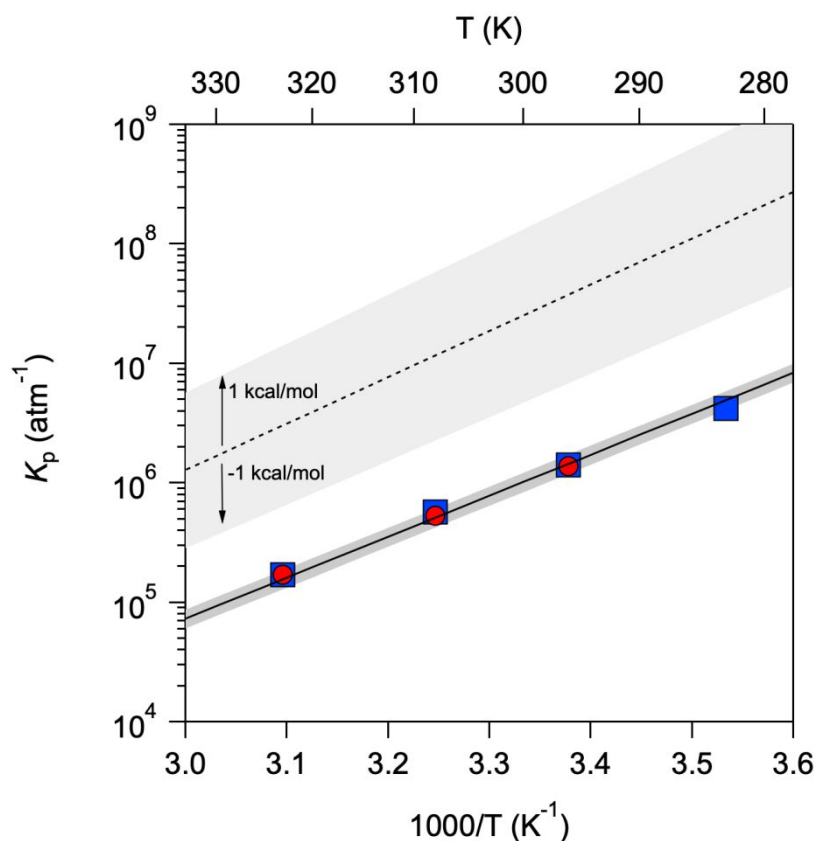


Fig. 4. $\text{Cl} + \text{C}_4\text{H}_2\text{O}_3 \leftrightarrow \text{Cl}\cdot\text{C}_4\text{H}_2\text{O}_3$ equilibrium constant data obtained in this work experimentally (symbols and solid line) and theoretically (dashed line) (see **Table 3**). The solid line is the third-law analysis of the combined N_2 (squares) and He (circles) data (see text). The shaded region around the experimental data represents the estimated uncertainty in the experimental measurement. The shaded region around the theoretically calculated value represents a 1 kcal mol^{-1} uncertainty in the reaction ΔH . The estimated accuracy of the calculation is $2\text{--}3 \text{ kcal mol}^{-1}$.

A second law analysis of the experimental $K_p(T)$ data yields $\Delta H = -14.5 \pm 0.4$ kcal mol⁻¹ and $\Delta S = -20.7 \pm 1.3$ cal mol⁻¹ K⁻¹. The uncertainty in ΔS is primarily due to the narrow temperature range of the experimental data.

Cl atoms could in principle react with maleic anhydride by abstraction of H from one of the C-H bonds, or by addition to one of the C=C or C=O pi bonds. At the CBS-QB3 level we compute that H abstraction is endothermic by 13 kcal mol⁻¹ and therefore is negligible in these experiments. Density functional theory revealed no bound adduct where Cl attacks a carbonyl group, by contrast to the OH + maleic acid system,¹⁴ and constraining the geometry to a plausible Cl-adduct leads to a CBS-QB3 energy around 10 kcal mol⁻¹ higher than the reactants, so again this channel may be neglected. See **Tables S3** and **S4** for calculated geometries and vibrational frequencies. For Cl addition to the C=C bond, our application of CBS-QB3 theory gave, for 298 K and with little dependence on T, $\Delta H = -17.7$ kcal mol⁻¹ and $\Delta S = -25.1$ cal mol⁻¹ K⁻¹ ($K_p(225\text{--}350\text{ K}) = 2.95 \times 10^{-6} T^{0.013} \exp(+8928/T)$) atm⁻¹. For comparison, G4 theory²⁶ yields $\Delta H = -18.6$ kcal mol⁻¹. Using density functional theory, there appears to be no barrier to this addition path.

The calculated parameters may be compared with the observed equilibrium between Cl atoms and maleic anhydride. The Second Law analysis for addition yields an entropy change that is 4.4 cal mol⁻¹ K⁻¹ and an enthalpy change that is 3.2 kcal mol⁻¹ more positive than calculated. This is within the observed range of deviations for CBS-QB3 theory,²³ but at the upper end. Use of the computed ΔS in a Third Law analysis yields an average ΔH of -15.7 kcal mol⁻¹ over the temperature range 280–330 K. The computed ΔH is still 2 kcal mol⁻¹ too negative, and this is the main factor leading to the greater calculated K_p values. A calculation using second order perturbation theory to compute anharmonic corrections in reactants and products, which tend to cancel, shows a shift in ΔS for adduct formation of +0.1 cal mol⁻¹ K⁻¹ and in ΔH of -0.04 kcal mol⁻¹, which are negligible. Therefore, the harmonic approximation is good for our purpose.

Cl•C₄H₂O₃ + O₂ rate coefficient

The rate coefficient for the reaction of the Cl•C₄H₂O₃ adduct with O₂, reaction 6, was measured at 296 K and 40 Torr (N₂ bath gas) total pressure. In these experiments, the MA concentration was held constant and the O₂ concentration was varied between $(4.97\text{--}51.7) \times 10^{13}$ molecule cm⁻³, i.e., pseudo first-order condition in Cl•C₄H₂O₃, in two separate experiments. **Figure 5** shows some of the measured Cl-atom temporal profiles. Representative profiles from the other dataset are shown

in the supporting information (**Figure S6**). The data show an increase in the Cl-atom loss at longer reaction time with increasing O₂ concentration. The Cl atom temporal profiles were analyzed as described earlier using eq. I. The fits are included in **Figure 5**.

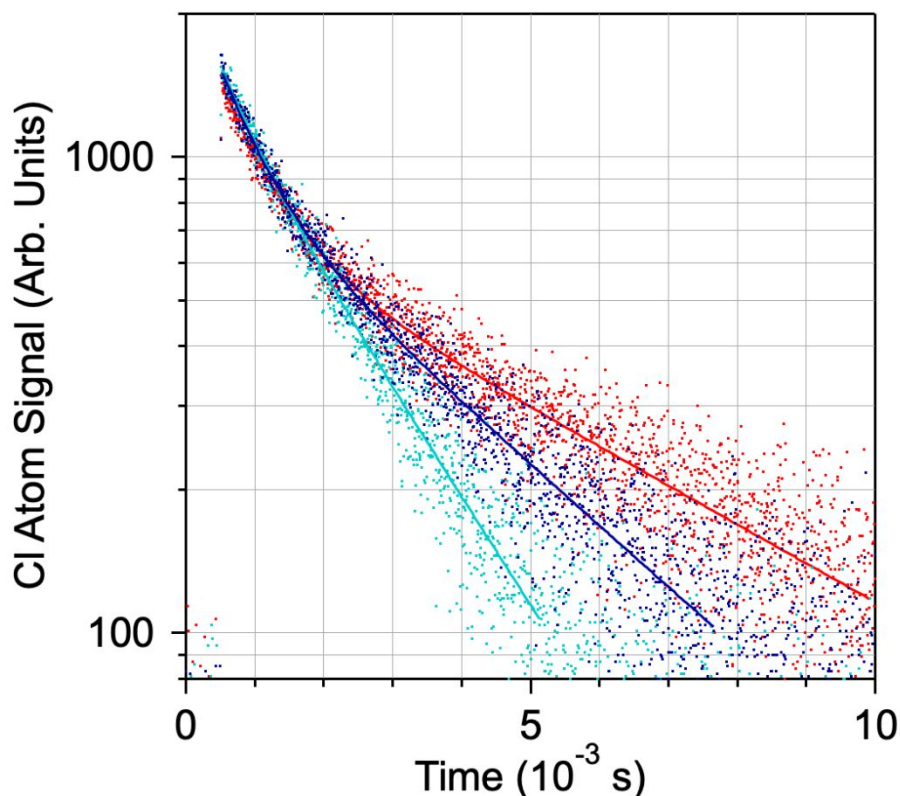


Fig. 5. Representative Cl atom temporal profiles obtained for a range of O₂ concentrations with a C₄H₂O₃ (MA) concentration of $(1.80 \pm 0.08) \times 10^{13}$ molecule cm⁻³ at 296 K and 40 Torr (N₂). O₂ concentrations from top to bottom profile are (10^{14} molecule cm⁻³): 0, 0.78, and 3.35. The lines are non-linear least-squares fits of the data to eq. I. Not all measured Cl atom profiles are shown for clarity, see **Figure 6**.

In our two experiments, the combined background loss of Cl and Cl•C₄H₂O₃ was measured to be 347 and 484 s⁻¹. A second-order plot of background loss corrected Cl•C₄H₂O₃ loss vs [O₂] is shown in **Figure 6**. The two experiments yield consistent results and a linear least-squares fit of the combined data yielded $k_6(296 \text{ K}) = (2.83 \pm 0.16) \times 10^{-12}$ cm³ molecule⁻¹ s⁻¹, where the quoted uncertainty is from the fit precision.

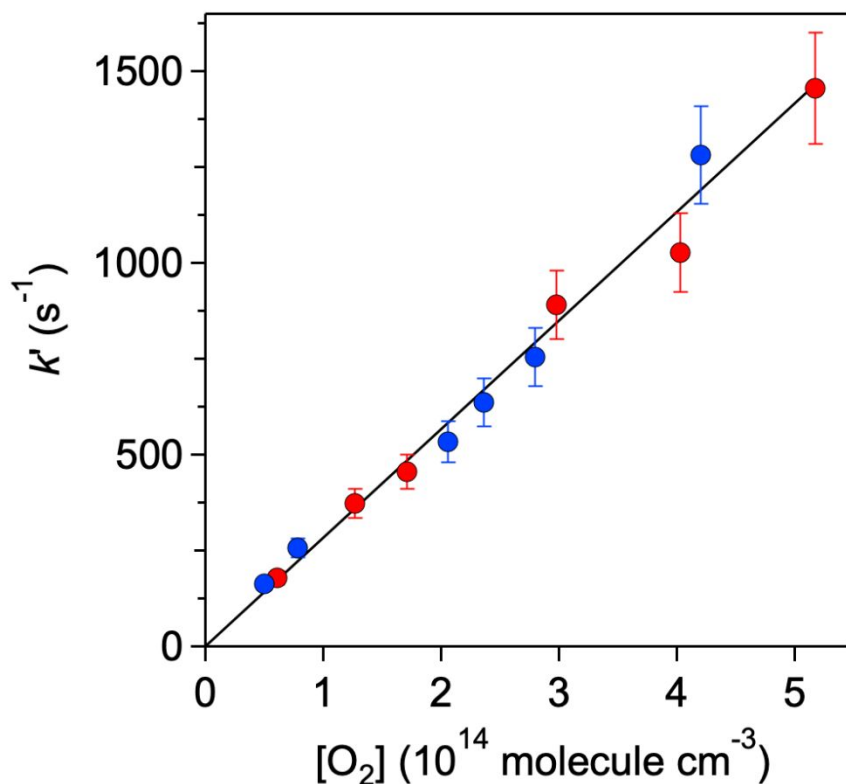


Fig. 6. Rate coefficient data (background loss corrected) obtained for the $\text{O}_2 + \text{Cl}\cdot\text{C}_4\text{H}_2\text{O}_3$ reaction, $k_6(296 \text{ K})$ at 40 Torr (N_2 bath gas). Independent measurements are represented by different colored symbols. The line is a linear least-squares fit of the combined data.

Reaction mechanism

An atmospheric MA degradation mechanism and the most likely stable end-products formed under high NO_x conditions following $\text{Cl}\cdot\text{C}_4\text{H}_2\text{O}_3$ adduct formation is outlined in **Figure 7**. Under atmospheric conditions, the carbon center radical will rapidly react with O_2 to form a peroxy radical, RO_2 . The subsequent RO_2 radical + NO reaction will lead to the formation of an alkoxy radical, RO . The ring opening unimolecular decomposition of the alkoxy radical may occur along two different pathways. That is, cleavage of the C-C bond adjacent to the carbonyl group or cleavage of the C-C bond of the original double bond. Our theoretical calculations predict that pathway A, cleavage of the C-C bond adjacent to the carbonyl group, is significantly energetically favored by $5.5 \text{ kcal mol}^{-1}$. The subsequent RO_2 chemistry along pathway A leads to the possible formation of chlorinated products formyl chloride (HC(O)Cl), glyoxyloxy chloride (HC(O)C(O)Cl), as well as glyoxal (HC(O)C(O)H), CO , and CO_2 . Pathway B would also lead to

the formation of HC(O)Cl , CO , and CO_2 with highly oxygenated carbonyl compounds also possible.

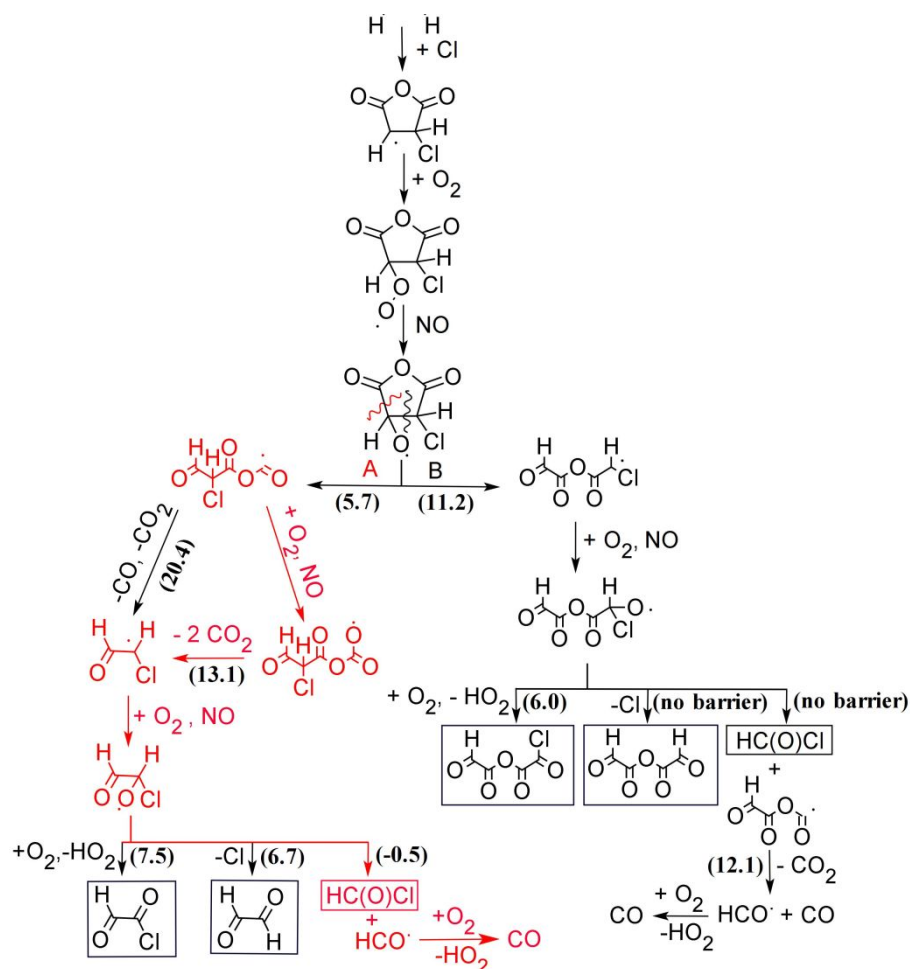


Fig. 7. Proposed maleic anhydride ($\text{C}_4\text{H}_2\text{O}_3$, MA) degradation mechanism and formation of stable end-products following the Cl -atom addition to the double bond. Quantities in parentheses are 0 K enthalpy barriers (kcal mol^{-1}) computed with CBS-QB3 theory. The theoretical and experimentally preferred pathway is given in red.

Reaction product yields

Product yield experiments were performed in a syn. air bath gas (630 Torr), i.e., in the absence of NO_x , such that RO radical formation was primarily due to RO_2 radical self-reaction. HC(O)Cl , CO , and CO_2 were observed as major reaction products. **Figure S7** shows representative infrared spectra obtained with a high initial MA concentration used to enhance product identification. HC(O)Cl was identified by its characteristic absorption bands centered at 738.6 and 1783.4 cm^{-1}

corresponding to the C-Cl and C=O stretch modes, respectively.²⁷⁻²⁹ A small amount of HCl was observed that presumably originates from the heterogeneous loss of HC(O)Cl and/or the Cl + HC(O)Cl reaction.^{28,30} No other reaction products were observed. According to the theoretically calculated reaction barriers given in **Figure 7**, other reaction products are possible, but expected to have negligible yields.

Figure 8 summarizes the results of four independent product yield experiments for the formation of HC(O)Cl, CO, and CO₂. The MA loss has been corrected for background loss as described earlier. The correction for background MA loss was ~11%. Note that the background loss of MA did not contribute to the formation of these products. Variations in the photolysis laser fluence, initial reactant concentrations, and reaction time did not affect the measured product yields. The total loss of MA due to reaction and background loss ranged between 62–100%. HC(O)Cl was quantified using the infrared cross section at 1793 cm⁻¹ of 1.63×10^{-18} cm² molecule⁻¹ reported by Wallington et al.³¹ The HC(O)Cl band at 738.6 cm⁻¹ (1.71×10^{-18} cm² molecule⁻¹) was used in our analysis due to spectral interference in the 1793 cm⁻¹ region. HC(O)Cl was semi-stable in the apparatus. We experimentally estimated the first-order rate coefficient for the dark loss of HC(O)Cl to be 8×10^{-4} s⁻¹. A ~6% correction was applied to the HC(O)Cl yield to account for dark loss. HC(O)Cl is reactive with Cl atoms, with a rate coefficient of 7.8×10^{-13} cm³ molecule⁻¹ s⁻¹,²⁸ although the experimentally measured HC(O)Cl profiles did not show evidence for reactive loss. The HC(O)Cl product yield was determined to be $(65 \pm 10)\%$, where the quoted uncertainty includes estimated uncertainty in the infrared analysis and MA and HC(O)Cl dark loss. The measured CO and CO₂ yields are (83 ± 7) and $(188 \pm 10)\%$, respectively. The carbon mass balance is shown in **Figure 8** and was $(86 \pm 16)\%$.

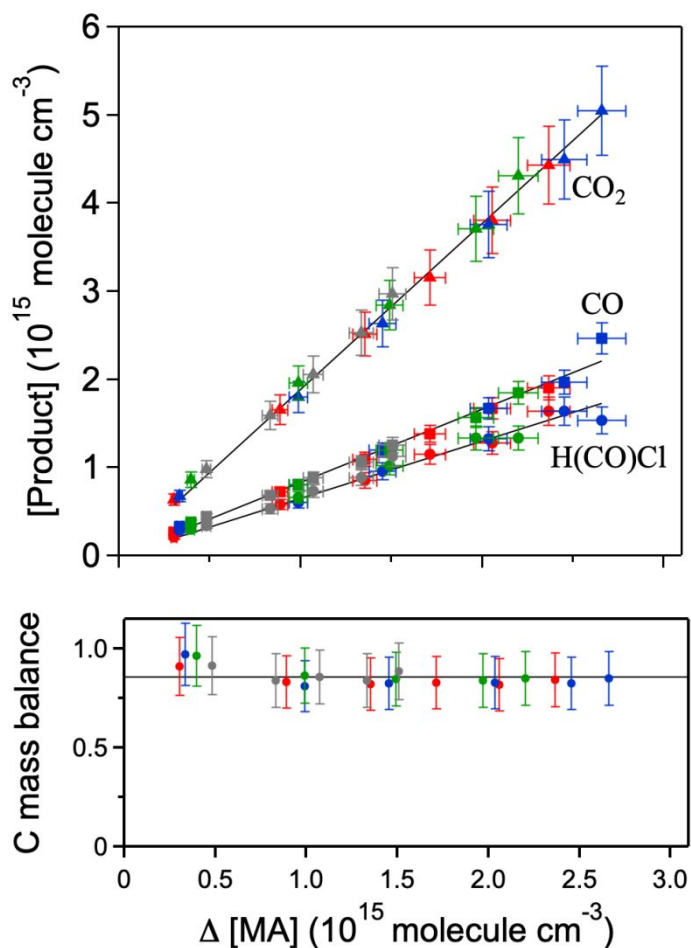


Fig. 8. Molar product yield data for the Cl initiated oxidation of $C_4H_2O_3$ (MA) reaction at 296 K in 630 Torr syn. air. Independent measurements performed under different experimental conditions are represented by different colored symbols. The lines are linear least-squares fits that give product yields of $(65 \pm 10)\%$ for HC(O)Cl, $(83 \pm 7)\%$ for CO, and $(188 \pm 10)\%$ for CO_2 , where the quoted uncertainty includes estimated systematic errors (see text). The lower panel shows the observed carbon mass balance. The line is the linear least-squares fit.

In summary, the measured CO_2 yield is close to 200%, which is most consistent with the mechanism following pathway A given in **Figure 7**. However, the measured CO_2 yield could allow for a small fraction of the MA degradation through pathway B. HC(O)Cl is expected to be a dominant reaction product (other than CO and CO_2) in degradation pathway A and also possibly in pathway B. This is because in pathway A the reaction barriers for products other than HC(O)Cl, i.e., glyoxyloxy chloride (HC(O)C(O)Cl) and glyoxal (HC(O)C(O)H) formation, have activation barriers calculated to be more than 7 kcal mol^{-1} greater. Along pathway B, other products are possible through near barrier less reactions. The experimentally measured product yield for

HC(O)Cl was less than 100%. There are several possible explanations for a value less than 100%. It could be that there is sufficient uncertainty in the literature reported infrared absorption cross section for HC(O)Cl, although previous yield studies from our laboratory³² would not support this explanation. There may also be systematic error in the corrections applied to the HC(O)Cl product yield, i.e., dark loss and reactive loss of HC(O)Cl as well as dark loss of MA, that may have been under-estimated. Finally, reaction products other than HC(O)Cl formed through pathway B, e.g. HC(O)C(O)OC(O)C(O)H, may not have been detected in our apparatus.

Conclusions

This study examined the gas-phase kinetics of the Cl atom + C₄H₂O₃ (maleic anhydride) reaction. Cl atom temporal profiles were measured in time resolved experiments over a range of temperature (283–323 K) and pressure (15–500 Torr, N₂ and He bath gases). The measurements demonstrated the formation of a Cl-C₄H₂O₃ semi-stable adduct as a reaction product. Analysis of the Cl atom profiles yielded reaction rate coefficient data that displayed a classical “fall-off” behavior consistent with such an association reaction mechanism. The following rate coefficient parameterization was derived from a fit to the experimentally observed rate coefficient data with a broadening coefficient, F_c , of 0.6:

$$k_0(T) = 9.4 \times 10^{-29} (T/298)^{-6.3} \quad \text{cm}^6 \text{ molecule}^{-2} \text{ s}^{-1}$$

$$k_\infty(T) = 3.4 \times 10^{-11} (T/298)^{-1.4} \quad \text{cm}^3 \text{ molecule}^{-1} \text{ s}^{-1}$$

where $k(298 \text{ K}, 760 \text{ Torr N}_2) = 3 \times 10^{-11} \text{ cm}^3 \text{ molecule}^{-1} \text{ s}^{-1}$. The collision efficiency of He was determined to be 0.34 that of N₂.

A third-law kinetic analysis yielded $K_p(283\text{--}323 \text{ K}) = 3.73 \times 10^{-6} \exp(7850/T)$ for the equilibrium of Cl and C₄H₂O₃ with the Cl-C₄H₂O₃ adduct, i.e., $\Delta S = -25.1 \text{ cal mol}^{-1} \text{ K}^{-1}$ and an average $\Delta H = -15.7 \text{ kcal mol}^{-1}$ over the temperature range 280–330 K.

The atmospheric lifetime of MA with respect to Cl reactive loss in the free troposphere, where the Cl atom concentration is estimated to be $\sim 1 \times 10^4 \text{ atom cm}^{-3}$, is estimated to be ~ 40 days. In the boundary layer or within a wildfire plume, the Cl atom concentration may be greater leading to a shorter MA lifetime. The MA lifetime with respect to OH reactive loss was estimated in our earlier study¹⁴ to be ~ 15 days. Therefore, Cl chemistry is likely to make a significant contribution to the overall lifetime of MA due to gas-phase reactive loss.

In addition to the possible significance of Cl atom chemistry on the atmospheric lifetime of MA, the atmospheric degradation of MA initiated by reaction with the Cl atom was shown to differ

primarily from OH radical initiated chemistry in the end-products formed. The reaction mechanism was examined in this study through product yield measurements and theoretical calculation of preferred reaction pathways and products. The degradation of MA was shown to lead to the formation of a temporary chlorine reservoir species, formyl chloride (HC(O)Cl), as a major stable end-product with a molar yield of $65 \pm 10\%$. The formation of HC(O)Cl and its gas-phase and heterogeneous atmospheric chemistry will impact chemical systems in locations remote to the MA emission source. The lessons learned in this study are, most likely, applicable to many other cyclic and heterocyclic unsaturated compounds that are emitted in biomass burning and wildfires. That is, chlorine initiated atmospheric chemistry will impact lifetimes and degradation products and may need to be considered in atmospheric model simulations.

ASSOCIATED CONTENT

Supporting Information

AUTHOR INFORMATION

Corresponding Author

*E-mail: James.B.Burkholder@noaa.gov (J.B.B.)

ORCID

J.B. Burkholder: [0000-0001-9532-6246](https://orcid.org/0000-0001-9532-6246)

Present address

Tomasz Gierczak, Department of Chemistry, Warsaw University, al. Zwirki i Wigury 101, 02-089 Warszawa, Poland

Vassileios C. Papadimitriou, Laboratory of Photochemistry and Chemical Kinetics, Department of Chemistry, University of Crete, Vassilika Vouton, 71003 Heraklion, Crete, Greece.

Conflicts of interest

The authors declare no competing financial interest.

Acknowledgements

This work was supported in part by NOAA Climate Program Office Atmospheric Chemistry, Carbon Cycle, and Climate Program and NASAs Atmospheric Composition Program. Computational facilities were provided through NSF grant CHE-1531468.

References

- 1 M. M. Coggon, C. Y. Lim, A. R. Koss, K. Sekimoto, B. Yuan, J. B. Gilman, D. H. Hagan, V. Selimovic, K. J. Zarzana, S. S. Brown, J. M. Roberts, M. Müller, R. Yokelson, A. Wisthaler, J. E. Krechmer, J. L. Jimenez, C. Cappa, J. H. Kroll, J. de Gouw and C. Warneke, *Atmos. Chem. Phys.*, 2019, **19**, 14875-14899.
- 2 M. Müller, B. E. Anderson, A. J. Beyersdorf, J. H. Crawford, G. S. Diskin, P. Eichler, A. Fried, F. N. Keutsch, T. Mikoviny, K. L. Thornhill, J. G. Walega, A. J. Weinheimer, M. Yang, R. J. Yokelson and A. Wisthaler, *Atmos. Chem. Phys.*, 2016, **16**, 3813-3824.
- 3 E. A. Bruns, J. G. Slowik, I. El Haddad, D. Kilic, F. Klein, J. Dommen, B. Temime-Roussel, N. Marchand, U. Baltensperger and A. S. H. Prévôt, *Atmos. Chem. Phys.*, 2017, **17**, 705-720.
- 4 A. Hartikainen, P. Yli-Pirilä, P. Tiitta, A. Leskinen, M. Kortelainen, J. Orasche, J. Schnelle-Kreis, K. E. J. Lehtinen, R. Zimmermann, J. Jokiniemi and O. Sipilä, *Environ. Sci. Technol.*, 2018, **52**, 4979-4988.
- 5 D. Grosjean, *J. Air Waste Manage. Assoc.*, 1990, **40**, 1664-1669.
- 6 G. Centi, F. Trifiro, J. R. Ebner and V. M. Franchetti, *Chem. Rev.*, 1988, **88**, 55-80.
- 7 V. V. Guliants and M. A. Carreon, *Catalysis: Volume 18. Vanadium-phosphorus-oxides: From fundamentals of n-Butane oxidation to synthesis of new phases*, The Royal Society of Chemistry, 2005.
- 8 J. Liu, Z. Du, Y. Yang, T. Lu, F. Lu and J. Xu, *ChemSusChem*, 2012, **5**, 2151-2154.
- 9 B. D. Roover, J. Devaux and R. Legras, *J Polym Sci A: Polym Chem*, 1996, **34**, 1195-1202.
- 10 E. Borrás and L. A. Tortajada-Genaro, *Atmos. Environ.*, 2012, **47**, 154-163.
- 11 J. F. Hamilton, A. C. Lewis, C. Bloss, V. Wagner, A. P. Henderson, B. T. Golding, K. Wirtz, M. Martin-Reviejo and M. J. Pilling, *Atmos. Chem. Phys.*, 2003, **3**, 1999-2014.
- 12 F. Villanueva, I. Barnes, E. Monedero, S. Salgado, M. V. Gómez and P. Martin, *Atmos. Environ.*, 2007, **41**, 8796-8810.
- 13 P. Marshall, V. C. Papadimitriou, D. K. Papanastasiou, J. M. Roberts and J. B. Burkholder, *J. Photochem. Photobiol. A*, 2019, **382**, 111953.
- 14 A. Chattopadhyay, V. C. Papadimitriou, P. Marshall and J. B. Burkholder, *Int. J. Chem. Kinet.*, 2020, **52**, 623-631.
- 15 B. Ghosh, D. K. Papanastasiou and J. B. Burkholder, *J. Chem. Phys.*, 2012, **137**, 164315.
- 16 D. K. Papanastasiou, K. J. Feierabend and J. B. Burkholder, *J. Chem. Phys.*, 2011, **134**, 204310.
- 17 J. M. Nicovich, S. Wang, M. L. McKee and P. H. Wine, *J. Phys. Chem.*, 1996, **100**, 680-688.
- 18 J. B. Burkholder, S. P. Sander, J. Abbatt, J. R. Barker, C. Cappa, J. D. Crouse, T. S. Dibble, R. E. Huie, C. E. Kolb, M. J. Kurylo, V. L. Orkin, C. J. Percival, D. M. Wilmouth and P. H. Wine, *Chemical Kinetics and Photochemical Data for Use in Atmospheric Studies*, Evaluation No. 19, JPL Publication 19-5, Jet Propulsion Laboratory, Pasadena, 2020 <http://jpldataeval.jpl.nasa.gov>.
- 19 J. A. Montgomery Jr, M. J. Frisch, J. W. Ochterski and G. A. Petersson, *J. Chem. Phys.*, 1999, **110**, 2822-2827.
- 20 R. D. Johnson III, NIST Computational Chemistry Comparison and Benchmark Database, release 21 (National Institute of Standards and Technology)

- 21 J. R. Barker, T. L. Nguyen, J. Stanton, C. Aieta, M. Ceotto, F. Gabas, T. J. D. Kumar, C. G. L. Li, L. L. Lohr, A. Maranzana, N. F. Ortiz, J. M. Preses, J. M. Simmie, J. A. Sonk and P. J. Stimac, MultiWell-2020, University of Michigan, Ann Arbor, MI: 2020, <http://aoss-research.engin.umich.edu/multiwell/>.
- 22 M. J. Frisch, G. W. Trucks, H. B. Schlegel, G. E. Scuseria, M. A. Robb, J. R. Cheeseman, G. Scalmani, V. Barone, G. A. Petersson, H. Nakatsuji, X. Li, M. Caricato, A. V. Marenich, J. Bloino, B. G. Janesko, R. Gomperts, B. Mennucci, H. P. Hratchian, J. V. Ortiz, A. F. Izmaylov, J. L. Sonnenberg, Williams, F. Ding, F. Lipparini, F. Egidi, J. Goings, B. Peng, A. Petrone, T. Henderson, D. Ranasinghe, V. G. Zakrzewski, J. Gao, N. Rega, G. Zheng, W. Liang, M. Hada, M. Ehara, K. Toyota, R. Fukuda, J. Hasegawa, M. Ishida, T. Nakajima, Y. Honda, O. Kitao, H. Nakai, T. Vreven, K. Throssell, J. A. Montgomery Jr., J. E. Peralta, F. Ogliaro, M. J. Bearpark, J. J. Heyd, E. N. Brothers, K. N. Kudin, V. N. Staroverov, T. A. Keith, R. Kobayashi, J. Normand, K. Raghavachari, A. P. Rendell, J. C. Burant, S. S. Iyengar, J. Tomasi, M. Cossi, J. M. Millam, M. Klene, C. Adamo, R. Cammi, J. W. Ochterski, R. L. Martin, K. Morokuma, O. Farkas, J. B. Foresman and D. J. Fox, Gaussian 16 Rev. A.03, Wallingford, CT, 2016.
- 23 K. P. Somers and J. M. Simmie, *J. Phys. Chem. A*, 2015, **119**, 8922-8933.
- 24 R. Atkinson, D. L. Baulch, R. A. Cox, J. N. Crowley, R. F. Hampson, R. G. Hynes, M. E. Jenkin, M. J. Rossi and J. Troe, *Atmos. Chem. Phys.*, 2006, **6**, 3625-4055.
- 25 A. Sharma, K. K. Pushpa, S. Dhanya, P. D. Naik and P. N. Bajaj, *Int. J. Chem. Kinet.*, 2010, **42**, 98-105.
- 26 L. A. Curtiss, P. C. Redfern and K. Raghavachari, *J. Chem. Phys.*, 2007, **126**, 084108.
- 27 I. C. Hisatsune and J. Heicklen, *Can. J. Spectrosc.*, 1973, **18**, 77.
- 28 H. Niki, P. D. Maker, C. M. Savage and L. P. Breitenbach, *Int. J. Chem. Kinet.*, 1980, **12**, 915-920.
- 29 G. Yarwood, H. Niki and P. D. Maker, *J. Phys. Chem.*, 1991, **95**, 4773-4777.
- 30 H. G. Libuda, F. Zabel, E. H. Fink and K. H. Becker, *J. Phys. Chem.*, 1990, **94**, 5860-5865.
- 31 T. J. Wallington, J. J. Orlando and G. S. Tyndall, *J. Phys. Chem.*, 1995, **99**, 9437-9442.
- 32 V. C. Papadimitriou, Y. G. Lazarou, R. K. Talukdar and J. B. Burkholder, *J. Phys. Chem. A*, 2011, **115**, 167-181.